IEEE Access
Multidisciplinary | Rapid Review | Open Access Journal

Received August 20, 2019, accepted September 8, 2019, date of publication September 12, 2019,
date of current version September 25, 2019.

Digital Object Identifier 10.1109/ACCESS.2019.2940758

Dynamic Trajectory Planning and Tracking for Autonomous Vehicle With Obstacle Avoidance Based on Model Predictive Control

SHAOSONG LI[1], ZHENG LI[1], ZHIXIN YU[1], BANGCHENG ZHANG[1], AND NIAONA ZHANG[2]
[1]School of Mechatronic Engineering, Changchun University of Technology, Changchun 130012, China
[2]School of Electrical and Electronic Engineering, Changchun University of Technology, Changchun 130012, China

Corresponding author: Bangcheng Zhang (zhangbangcheng@ccut.edu.cn)

This work was supported in part by the National Natural Science Foundation of China under Grant 51905045, in part by the Key Technology on Major Program of Jilin Province under Grant 20170201005GX, and in part by the Science and Technology Research Planning Project of the Education Department of Jilin Province under Grant JJKH20181035KJ.

ABSTRACT In this study, an obstacle avoidance controller based on nonlinear model predictive control is designed in autonomous vehicle navigation. The reference trajectory is predefined using a sigmoid function in accordance with road conditions. When obstacles suddenly appear on a predefined trajectory, the reference trajectory should be adjusted dynamically. For dynamic obstacles, a moving trend function is constructed to predict the obstacle position variances in the predictive horizon. Furthermore, a risk index is constructed and introduced into the cost function to realize collision avoidance by combining the relative position relationship between vehicle and obstacles in the predictive horizon. Meanwhile, lateral acceleration constraint is also considered to ensure vehicle stability. Finally, trajectory dynamic planning and tracking are integrated into a single-level model predictive controller. Simulation tests reveal that the designed controller can ensure real-time trajectory tracking and collision avoidance.

INDEX TERMS Autonomous vehicle, dynamic obstacles, moving trend function, dynamic planning and tracking, single-level controller.

I. INTRODUCTION

With the rapid development of technology in the 21st century, autonomous vehicles have become an attainable reality [1]. They have attracted widespread attention because of the continuous improvement of automatic driving levels [2], [3]. However, with the improvement of automation level, road traffic accidents occur frequently in recent years [4]. Safety has become the eternal theme of autonomous vehicles [5], [6].

Active collision avoidance system can effectively improve traffic safety, and has become a research hotspot in the field of automotive active safety. In literature [7], distributed controllers were designed to avoid collisions between a group of underactuated ships. Literatures [8] and [9] presented a formation maneuver control method to avoid collisions between each vehicle and its front vehicles. For autonomous vehicles, obstacle avoidance refers to perceiving environmental information and generating control commands to navigate a vehicle around obstacles safely [10]–[12]. It can be roughly divided into the following four steps: environmental identification and integration, behavioral decision, trajectory planning, and trajectory tracking. Among these steps, trajectory planning and tracking are important control segments [13]. Real-time planning and tracking feasible trajectories are necessary for autonomous vehicle driving [14].

Many research methods have been used for the trajectory planning and tracking of autonomous vehicles. The reinforcement learning approach is widely applied to autonomous vehicles and robots for trajectory planning or obstacle avoidance. Such application can usually ensure safety by mastering a complete state and environment knowledge after experiencing failures during training time [15], [16]. However, this method still requires a lot of training and test data, and the implementation is complex and costly. An artificial potential field method is used to generate repulsive potential fields to obstacles and attractive potential fields to the goal. Using this method, vehicles can avoid collisions with obstacle boundaries while proceeding toward their goals [17]. However, existing local minimum problems in this method may prevent vehicles from arriving at their targets.

Model predictive control (MPC) is an attractive method due to its flexibility and ability to compute optimal solutions with hard and soft constraints [18], [19]. It has the abilities

The associate editor coordinating the review of this manuscript and approving it for publication was Heng Zhang.

of predicting the future dynamics of a system and receding horizon optimization [20], [21]. Thus, MPC is a natural candidate for the trajectory planning and tracking of an autonomous vehicle in obstacle avoidance [22]. Most of existing obstacle avoidance controllers are designed on the basis of hierarchical architecture. In hierarchical controllers, the higher level is a path planner, whereas the lower level is a path tracker. Gao proposed a hierarchical obstacle avoidance control architecture in literatures [14], [23]–[25]. In his literatures, the path reference values obtained by the upper level re-planning controller were sent to the lower level for path tracking. However, the high-level path planner may generate dynamic infeasible trajectories in this case [26]. In addition, collisions with obstacles may occur if the vehicle deviates from the reference track. Compared with the hierarchical controller, the single-level controller integrates trajectory planning and tracking in one level. This structure can usually avoid the generation of inactive dynamic trajectories at the upper level. In literatures [10]–[12], [26]. Liu presented an obstacle avoidance algorithm that combines path planning and tracking into a single-level architecture. In Literature [27], a simultaneous trajectory planning and tracking controller is presented to address obstacle avoidance. Meanwhile, the selection of discrete time is crucial for single-level controllers. A long discrete time is always expected to predict further in favor of collision avoidance. However, the discrete time should still be as small as possible to ensure smooth control action in tracking control. To solve this contradiction effectively, Literatures [13], [28], [29] presented the strategy of varying discrete steps and realized the good effects of tracking and collision avoidance.

In a practical environment, dynamic obstacles may appear on the desired path. If the actual vehicle trajectory is not dynamically adjusted, then the vehicle may collide with obstacles in the course of trajectory tracking. This condition depends on whether the future motion trend of a dynamic obstacle can be predicted effectively [30]–[32]. Risk can be predicted by combining the future status of vehicle and obstacles to adjust the trajectory dynamically. Relative studies on avoiding moving obstacles based on MPC have also progressed. In literature [33], a collision-free navigation function was designed for real-time collision avoidance of autonomous vehicles in static and dynamic environments. The proposed approach is applicable to point obstacles and also has good compatibility with lidar point clouds. In literatures [34] and [35], a hierarchical predictive trajectory guidance and control framework was proposed in consideration of moving obstacles in predictive horizon with an elliptical constraint. In literature [36], an integrated controller was designed to realize adaptive cruise control coupled with obstacle avoidance. In this literature, the distance between an eGO vehicle and a moving object was considered in the predictive horizon in accordance with their motion states at the beginning of the horizon.

In this study, an integrated controller considering simultaneous dynamic planning and tracking is designed. The reference trajectory is predefined using a sigmoid function. For appearing dynamic obstacles that threaten the vehicle trajectory, a moving trend function is structured to predict the position of the obstacles in the predictive horizon. Then, the reference trajectory is adjusted dynamically by combining the predicted vehicle and dynamic obstacles in the predictive horizon with a nonlinear model predictive control (NMPC). The proposed controller controls the vehicle to realize obstacle avoidance and path tracking by optimizing the front steering angle. Different from literature [36], a method of varying discrete steps is adopted in this paper to compatible with path tracking and obstacle avoidance better. At the same time, lateral acceleration constraint is also considered in the optimization.

The remainder of this paper is organized as follows: In Section II, the whole control flow of the proposed controller is described. In Section III, the generation of reference trajectory based on the sigmoid function is stated. In Section IV, the 2-DOF bicycle model and the Pacejka tire model for controller design are introduced. The collision avoidance with dynamic obstacle is discussed in Section V. In Section VI, the problem of optimization solution is obtained. In Section VII, simulations conducted under different operating conditions are reported. Finally, in Section VIII, the conclusions are presented.

II. CONTROL FRAME

The whole control process is shown in Figure 1. The reference trajectory is predefined using a sigmoid function in accordance with road environment information. The desired yaw angle and lateral displacement obtained by the sigmoid function are sent to the NMPC controller for collision avoidance. When new obstacles appear on the predefined reference trajectory, a lidar unit mounted on the vehicle can detect their position information. To realize collision avoidance effectively, a moving trend function is established to reflect the position changes of point obstacles in the predictive horizon. In accordance with the position changes of the vehicle and the obstacles at each step in the predictive horizon, a risk index is built and imposed to the controller. In keeping with the given information, the front steering angle is optimized by the controller to navigate the vehicle safely. Vehicle state information is fed back to the prediction model to achieve continuous dynamic planning and tracking control. At the same time, the lateral acceleration constraint is considered in the optimization to ensure vehicle stability. Finally, an integrated control process for simultaneous dynamic planning and tracking is formed.

III. GENERATION OF REFERENCE TRAJECTORY

When a static obstacle or a forbidden area is in front of the vehicle, a safe avoidance trajectory should be generated to complete a safe lane-changing operation. A good avoidance trajectory not only needs to ensure safe and collision-free driving but must also consider driving comfort and real-time updating characteristics of the trajectory.

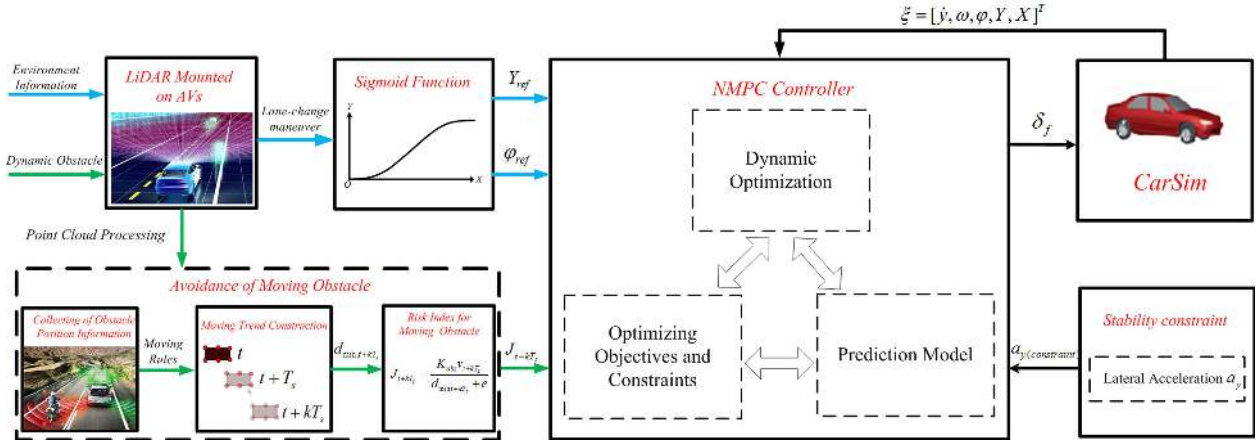

FIGURE 1. Control flow of the integrated controller.

Therefore, the following conditions should be followed in setting the reference trajectory:

- Free from collision with obstacles;
- Satisfied vehicle dynamic constraints;
- Smooth trajectory curvature without sudden change;
- Simple trajectory equation that can be quickly updated.

The common planning methods used for reference trajectory include half arc and line matching, sine or cosine function, trapezoid function based on lateral acceleration, etc. However, they don't consider vehicle dynamics constraints and the smooth transition of curve simultaneously. Compared with these traditional methods, the sigmoid function has the following advantages: Firstly, the expression form is relatively simple, and only three parameters need to be adjusted. Secondly, the curve is continuous, which can avoid the problem of curvature mutation. Finally, vehicle dynamics constraints are considered.

In view of the above considerations, the reference trajectory is predefined using the sigmoid function. As shown in Figure 2, Y_{tol} is an additional parameter which represents the starting point of the lateral displacement of the vehicle. The expression of the sigmoid function is as follows:

$$Y(X)=\frac{B}{1+e^{-A(X-C)}} \tag{1}$$

where X and Y are the abscissa and ordinate of the vehicle centroid in the geodetic coordinate, respectively, which can be determined by using GPS and electronic map; A is the slope of the curve midpoint, which can represent the urgency of avoidance; B is the maximum lateral avoidance distance;

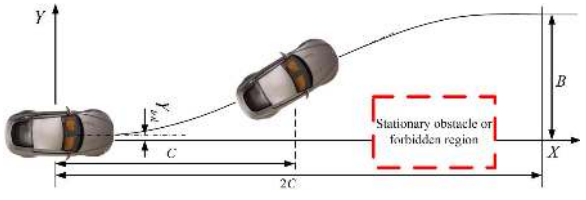

FIGURE 2. Reference trajectory based on the sigmoid function.

$2C$ is the total longitudinal distance between the vehicle and the target point.

In sigmoid function, the maximum lateral acceleration and jerk constraints can be taken into account simultaneously in determining parameter A. The corresponding inequality expressions are as follows:

$$|a_y(X)| \le a_{y\max} \tag{2a}$$
$$|j(X)| \le j_{\max} \tag{2b}$$

where $a_{y\max}$ is the maximum lateral acceleration, which can represent the lateral stability of vehicle; $j_{\max}$ indicates the maximum lateral jerk, which can reflect driver's comfort.

When a vehicle is traveling at a speed of U_0, parameter A can be obtained preliminarily considering the maximum lateral acceleration. And the specific expression is as follows:

$$A_{ay}=-\frac{(\rho_1+1)^2\sqrt{-\rho_1 B\rho_2 a_{y\max}}}{\rho_1 B\rho_2}$$
$$s.t.$$
$$\rho_1=\sqrt{2}\frac{s_2}{\sqrt{s_1}}(6U_0^2+2a_{y\max}B+\frac{4a_{y\max}^2B^2}{3U_0^2})+\frac{2a_{y\max}B}{3U_0^2}+1$$
$$\rho_2=a_{y\max}\rho_1 B-U_0^2\rho_1^2+U_0^2$$
$$s_1=9U_0^4+3a_{y\max}BU_0^2+2a_{y\max}^2B^2$$
$$s_2=\cos(\frac{1}{3}\tan^{-1}(\frac{3U_0^2\sqrt{81U_0^8+27U_0^4s_3^2+3s_3^4}}{27U_0^6+9U_0^2s_3^2+4s_3^3+27U_0^4s_3}))$$
$$s_3=a_{y\max}B \tag{3}$$

Meanwhile, the maximum lateral jerk constraint should also be considered. The specific expression is as follows:

$$A_j=\frac{1}{6U_0^3}(\sqrt[3]{s_4}+\frac{B^2j_{\max}^2}{\sqrt[3]{s_4}}+Bj_{\max})$$
$$s.t.$$
$$s_4=\frac{j_{\max}}{B}(86U_0^6+B^4j_{\max}^2+24U_0^3\sqrt{1296U_0^6+3B^4j_{\max}^2}) \tag{4}$$

Finally, the smaller value obtained by the two methods is taken as the final value of parameter A:

$$A = \min(A_{ay}, A_j) \tag{5}$$

When parameters A and B are determined, parameter C can be calculated as follows:

$$C = \frac{1}{A} \ln \frac{B - Y_{tol}}{Y_{tol}} \tag{6}$$

More detailed calculations of parameters A, B and C can be found in literature [37].

When a vehicle needs to complete lane-changing operation, the maximum lateral avoidance distance B should be determined on the basis of the safety position to be reached. In order to consider both vehicle stability and driver's comfort during lane-changing maneuver, the maximum lateral acceleration and jerk are adopted to determine the slope A of the curve midpoint. Meanwhile, the total longitudinal distance $2C$ should also be confirmed to ensure when the lane-changing maneuver is completed.

In trajectory tracking, the deviations between actual yaw angle, lateral displacement and reference are commonly used to evaluate tracking performance. In this study, the reference trajectory can be dissociated into several desired lateral displacement and yaw angle values. The specific approach is shown in Figure 3.

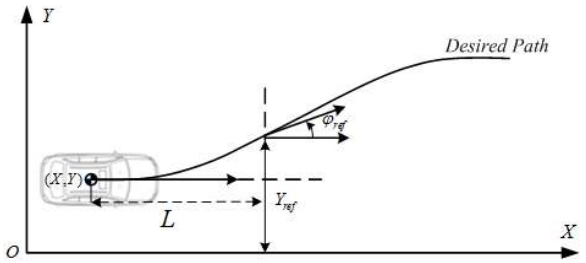

FIGURE 3. Desired yaw angle and displacement obtained from the reference trajectory.

In Figure 3, L is the preview distance, which is determined in accordance with the curvature of the road and longitudinal velocity. The specific determination method can be found in literature [38]. Y_{ref} is the reference lateral displacement, and φ_{ref} stands for the reference yaw angle. The expression can be written as follows:

$$Y_{ref}(X + L) = \frac{B}{1 + e^{-A(X+L-C)}} \tag{7a}$$

$$\varphi_{ref}(X + L) = \frac{d[Y_{ref}(X + L)]}{dX} \tag{7b}$$

IV. ESTABLISHMENT OF MODELS

In this part, the vehicle dynamic and tire models are introduced for controller design. In Section *A*, the 2-DOF kinematic and dynamic bicycle model is introduced. Meanwhile, in Section *B*, the Pacejka tire model is used to describe tire lateral force.

A. VEHICLE MODEL

For model predictive control, the precision of the selected model can directly affect the control effect. An accurate model can improve control accuracy but increase the computational burden of a system.

In consideration of the real-time operation and accuracy of the control system, the 2-DOF bicycle model is suitable for collision avoidance, which can be referred in literatures [39] and [40]. As shown in Figure 4, the following assumptions are mentioned:

- The longitudinal velocity of vehicle is constant;
- The left and right wheels on the same axle are simplified as one wheel;
- Only the lateral and yaw motion of the vehicle are considered.

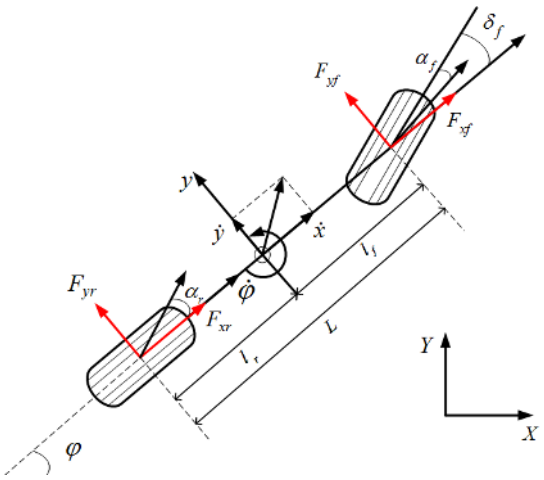

FIGURE 4. Vehicle model for control design.

The dynamic equation can be expressed as:

$$\ddot{y} = \left(F_{yf} + F_{yr}\right)/m - U_0\omega \tag{8a}$$

$$\dot{\omega} = \left(l_f F_{yf} - l_r F_{yr}\right)/I_z \tag{8b}$$

$$\dot{\varphi} = \omega \tag{8c}$$

$$\dot{Y} = U_0 \sin\varphi + \dot{y}\cos\varphi \tag{8d}$$

$$\dot{X} = U_0 \cos\varphi - \dot{y}\sin\varphi \tag{8e}$$

where $\dot{y}$ and $\ddot{y}$ are the lateral velocity and acceleration of vehicle, respectively; F_{yf} and F_{yr} represent the lateral forces of the front and rear axles, respectively; m and U_0 indicate the constant mass and longitudinal velocity of the vehicle, respectively; φ is the yaw angle of the vehicle; $\dot{\varphi}$ and $\dot{\omega}$ stand the yaw rate and yaw acceleration of the vehicle, respectively; l_f and l_r are the distances from the vehicle's center of mass to the front and rear axles, respectively; I_z denotes the rotational inertia of the vehicle; $\dot{X}$ and $\dot{Y}$ are the longitudinal and lateral velocity of the vehicle centroid in the geodetic coordinate system, respectively.

The dynamic model can be written as a nonlinear function:

$$\dot{\xi}(t) = f^{N2DOF}\left(\xi(t), u(t)\right) \tag{9a}$$

$$y_c(t) = \eta\xi(t) \tag{9b}$$

where

$$\xi(t) = \begin{bmatrix} \dot{y} \\ \omega \\ \varphi \\ Y \\ X \end{bmatrix} \quad u(t) = [\delta_f]$$

$$\eta = [0 \quad 0 \quad 1 \quad 1 \quad 0] \quad y_c(t) = \begin{bmatrix} \varphi \\ Y \end{bmatrix}$$

where $\xi(t)$ and $u(t)$ are the vehicle states and control input of the system, respectively; $y_c(t)$ is the predicted output of the system; η is the coefficient matrix, which can determine the number of predicted outputs. The system has five state variables, one control input, and two predicted outputs. The five state variables include vehicle lateral velocity, yaw rate, yaw angle, and lateral and longitudinal displacements in the geodetic coordinate system. The system input is the front steering angle δ_f. The predicted outputs are the yaw angle φ and lateral displacement Y of vehicle.

B. TIRE MODEL

When tire slip angle is small, tire lateral force has a linear relationship with slip angle. However, when tire slip angle exceeds a certain value, the relationship between slip angle and lateral force becomes nonlinear. In this study, the Pacejka tire model is used to reflect the nonlinear characteristics of tire force and is expressed as follows:

$$F_y = \mu D_y \sin(C_y \arctan(B_r - E_y(B_r - \arctan B_r))) \quad (10)$$

where

$$\begin{aligned} B_r &= B_y - \alpha \\ C_y &= a_0 \\ D_y &= a_1 F_z^2 + a_2 F_z \\ B_y &= \frac{a_3 \sin(2 \arctan(F_z/a_4))}{C_y D_y} \\ E_y &= a_5 F_z + a_6 \end{aligned}$$

where F_y is the tire lateral force, and α is the tire slip angle. B_y, C_y, D_y, and E_y depend on the normal force of the tire, where $a_0 = 1.75$, $a_1 = 0$, $a_2 = 1000$, $a_3 = 1289$, $a_4 = 7.11$, $a_5 = 0.0053$, and $a_6 = 0.1952$.

Tire lateral force and slip angle under different adhesion coefficients and vertical loads are shown in Figures 5(a) and 5(b), respectively.

The tire slip angles are defined as:

$$\alpha_f = \arctan(\frac{\dot{y} + \dot{\varphi} l_f}{U_0} - \delta_f) \quad (11a)$$

$$\alpha_r = \arctan(\dot{y} - \dot{\varphi} l_r) \quad (11b)$$

F_z is the total vertical load of the vehicle, which is distributed between the front and rear axles on the basis of the geometry of the vehicle model (described by parameters l_f and l_r):

$$F_{zf} = \frac{mgl_r}{l_f + l_r} \quad (12a)$$

$$F_{zr} = \frac{mgl_f}{l_f + l_r} \quad (12b)$$

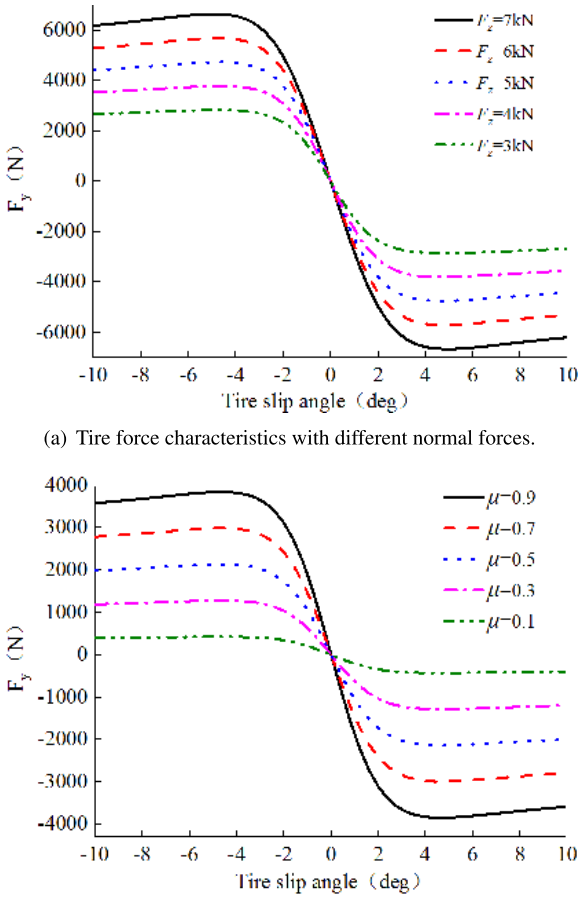

(a) Tire force characteristics with different normal forces.

(b) Tire force characteristics with different road adhesion coefficients.

FIGURE 5. Tire force characteristics.

V. DETECTION AND AVOIDANCE FOR DYNAMIC OBSTACLES

In Section III, a sigmoid function is predefined as the reference trajectory. However, when dynamic obstacles appear on the predefined trajectory, the reference trajectory may be threatened. In this case, the vehicle may collide with dynamic obstacles. Therefore, the reference trajectory should be dynamically adjusted. Moreover, the vehicle should be controlled to track the adjusted safety trajectory.

A. POSITION DETECTION OF DYNAMIC OBSTACLES

Obstacle position information is usually detected by lidar. Performing lidar on an autonomous vehicle can obtain the absolute distance to the border of obstacle. Obstacle position information can be described by lidar point clouds. Thus, obstacles are discretized into several points (pX_j, pY_j), as shown in Figure 6.

Normally, the lidar mounted on vehicle can measure the distance r_m to obstacle and the angle θ between obstacle and X-axis of vehicle coordinate system. If the distance r_m and angle θ have been obtained, the obstacle position (pX_j, pY_j) in the geodetic coordinate system can be calculated by

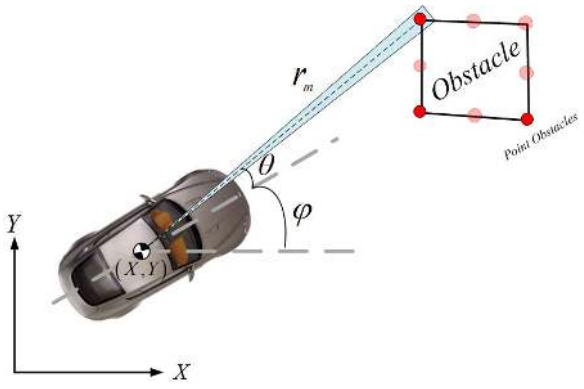

FIGURE 6. Position detection of the point obstacles.

coordinate transformation:

$$\begin{cases} pX_j = r_m \cos(\theta + \varphi) + X \\ pY_j = r_m \sin(\theta + \varphi) + Y \end{cases} \tag{13}$$

where X and Y are the longitudinal and lateral position of vehicle in the geodetic coordinate system.

B. MOVING TREND ESTABLISHMENT FOR OBSTACLES

In model predictive control, vehicle states in the predictive horizon can be predicted in accordance with current feedback information from the vehicle. However, the obstacle information can be only acquired by a lidar point at each sample time rather than in the predictive horizon. Collision avoidance is an urgent process, the future states of the vehicle and the obstacles should be all predicted to realize safe driving.

A moving trend function is constructed to predict point obstacle position in the predictive horizon. During an MPC predictive horizon, all objects are assumed to move with the speeds and accelerations at the beginning of the horizon. Literatures [27], [33] and [34] also adopted similar methods to predict the position of obstacles in the predictive horizon. Better obstacle avoidance effects were achieved in these literatures.

If the position of a point obstacle detected by lidar is $(pX_{j,t}, pY_{j,t})$ at time t, then its position coordinate in the predictive horizon is as follows:

$$\begin{cases} pX_{j,t+kT_s} = pX_{j,t+(k-1)T_s} + \rho_x \\ \quad k = 1, 2, \cdots\cdots, P \\ pY_{j,t+kT_s} = pY_{j,t+(k-1)T_s} + \rho_y \\ \quad k = 1, 2, \cdots\cdots, P \end{cases} \tag{14}$$

where

$$\rho_x = \begin{cases} p\dot{X}_{j,t}T_s & \textit{Uniform Speed} \\ p\dot{X}_{j,t+(k-1)T_s}T_s + \dfrac{1}{2}p\ddot{X}_{j,t}T_s^2 & \textit{Variable Speed} \\ \quad k = 1, 2, \cdots\cdots, P \end{cases}$$

$$\rho_y = \begin{cases} p\dot{Y}_{j,t}T_s & \textit{Uniform Speed} \\ p\dot{Y}_{j,t+(k-1)T_s}T_s + \dfrac{1}{2}p\ddot{Y}_{j,t}T_s^2 & \textit{Variable Speed} \\ \quad k = 1, 2, \cdots\cdots, P \end{cases}$$

where P represents the predictive horizon; T_s represents the predictive step size in the predictive horizon; $p\dot{X}_{j,t}$ and $p\dot{Y}_{j,t}$ are the longitudinal and lateral speed of a moving obstacle at time t, respectively; $p\ddot{X}_{j,t}$ and $p\ddot{Y}_{j,t}$ are the longitudinal and lateral acceleration of a moving obstacle at time t, respectively.

C. RISK INDEX DESIGN FOR COLLISION AVOIDANCE

A risk index between the vehicle and the point obstacles is designed to avoid dynamic obstacles effectively in trajectory tracking. The risk index is imposed into a cost function to optimize the front steering angle, thereby realizing collision avoidance.

In Figure 7, l_f, l_r, and c are the external dimensions of the vehicle. c denotes half the width of the vehicle. Then, j points are acquired at the edge of obstacle at each predictive step, which are marked as $\left(pX_{t+kT_s,j}, pY_{t+kT_s,j}\right)$. If these points are predicted in the geodetic coordinate, they can be transformed into the vehicle body frame as follows:

$$\begin{aligned} D_{x,j,t+kT_s} &= \left(pY_{t+kT_s,j} - Y_{t+kT_s}\right)\sin\varphi_{t+kT_s} \\ &\quad + \left(pX_{t+kT_s,j} - X_{t+kT_s}\right)\cos\varphi_{t+kT_s} \end{aligned} \tag{15a}$$

$$\begin{aligned} D_{y,j,t+kT_s} &= \left(pY_{t+kT_s,j} - Y_{t+kT_s}\right)\cos\varphi_{t+kT_s} \\ &\quad - \left(pX_{t+kT_s,j} - X_{t+kT_s}\right)\sin\varphi_{t+kT_s} \end{aligned} \tag{15b}$$

The minimum distance to all obstacle points is defined as $d_{\min,t+kT_s}$ in the predictive horizon, which can be determined by the following segmentation function:

$$\begin{aligned} &\textit{Case } 1 \\ &\textit{if } D_{y,j,t+kT_s} \in [-c, c] \textit{ and } D_{x,j,t+kT_s} > l_f; \\ &\quad d_{\min,t+kT_s} = \min(D_{x,j,t+kT_s} - l_f) \\ &\textit{Case } 2 \\ &\textit{if } D_{y,j,t+kT_s} \in [-c, c] \textit{ and } D_{x,j,t+kT_s} \in [-l_r, l_f]; \\ &\quad d_{\min,t+kT_s} = 0 \\ &\textit{Case } 3 \\ &\textit{if other conditions} \\ &\quad d_{\min,t+kT_s} = \inf \end{aligned} \tag{16}$$

where *inf* is a sufficiently large number.

In order to further elaborate the significance of equation (16), the scenarios of the three segmented functions are illustrated graphically in Figure 8.

In *Case* 1, the host vehicle has a certain distance from the obstacles. In this case, the minimum deviation $D_{x,j,t+kT_s}$ between the abscissas of point obstacle in a vehicle body frame and the body size is taken as the minimum distance.

In *Case* 2, the host vehicle overlaps with the obstacles and the abscissas of point obstacles in a vehicle body frame is in the range of $[-l_r, l_f]$. In this case, the host vehicle will collide with the obstacle. The value of the minimum distance $d_{\min,t+kT_s}$ is set to be zero.

In other conditions, the value of $d_{\min,t+kT_s}$ is set to be a sufficiently large value to disregard obstacles that do not lie within the vehicle's line of sight.

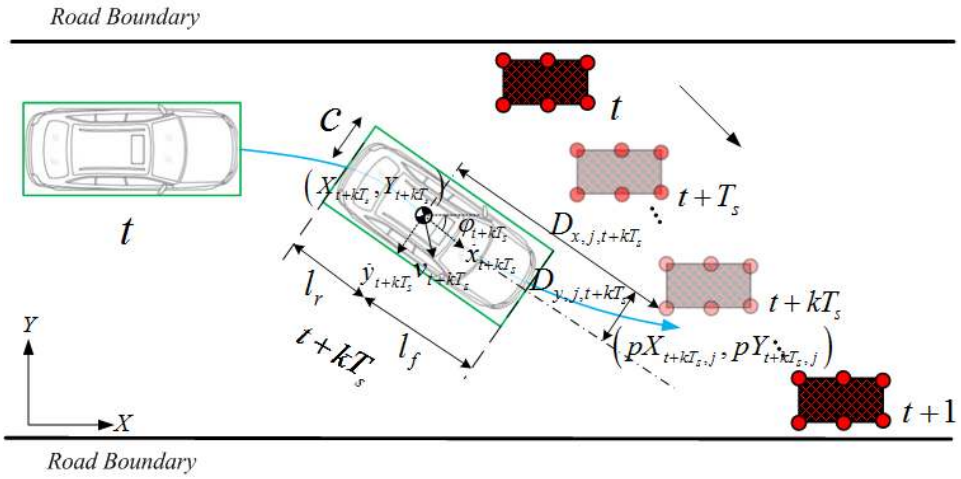

FIGURE 7. Schematic of obstacle dangerous distance.

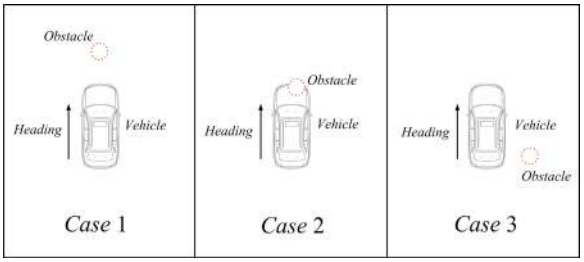

FIGURE 8. The diagram of segmented functions.

Thus, the risk index is defined as follows in the predictive horizon:

$$J_{t+kT_s} = \frac{K_{obs} v_{t+kT_s}}{d_{\min,t+kT_s} + e} \tag{17}$$

where K_{obs} is an adjustable weight coefficient. When the value of K_{obs} increases, the value of risk index J_{t+kT_s} will become larger. It means that the risk index accounts for a larger proportion in the cost function. In this case, the effect of obstacle avoidance will be more obvious in the process of optimizing. v_{t+kT_s} is the vehicle speed at each step in the predictive horizon, which can be expressed as $v^2_{t+kT_s} = \dot{x}^2_{t+kT_s} + \dot{y}^2_{t+kT_s}$; e is a small number, which is used to prevent the denominator from being zero. The smaller the closest distance $d_{\min,t+kT_s}$ is, the greater the risk index J_{t+kT_s} is. Therefore, collisions are likely to happen.

VI. OPTIMIZATION SOLUTION

In this section, the cost function is constructed. Meanwhile, the corresponding stability constraint is also considered to achieve effective collision avoidance. Accordingly, the flow diagram of the whole algorithm used for obstacle avoidance is presented in Figure 9.

Firstly, parameters A, B, and C are initialized to determine the sigmoid function as the reference trajectory. The vehicle is then controlled to track this trajectory. Afterwards, the reference trajectory is checked if new obstacles appear as a threat. If no obstacle is found, the vehicle will continue to follow the reference trajectory. Otherwise, a risk index will be structured into the cost function for obstacle avoidance. Finally, the optimal solution can be obtained.

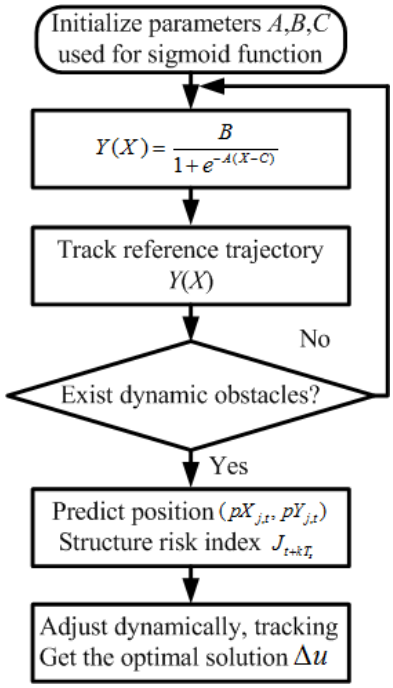

FIGURE 9. Flow diagram of the obstacle avoidance algorithm.

A. COST FUNCTION DESIGN

Equation (9a) is discretized with a fixed sampling time T_s. The discrete model of equation (9a) can be expressed as follows:

$$\xi(k) = f^{N2DOF}(\xi(k), u(k)) \tag{18a}$$
$$g(\Delta u(k)) = u(k) - u(k-1) \tag{18b}$$
$$y_c(k) = C\xi(k) \tag{18c}$$

At each predictive step, the state variable can be expressed as follows:

$$\begin{aligned} x(k+1\,|k\,) &= f(x(k),\ g(\Delta u(k))) \\ x(k+2\,|k\,) &= f(x(k+1),\ g(\Delta u(k+1))) \\ &= f(f(x(k),\ g(\Delta u(k))),\ g(\Delta u(k+1))) \\ &\vdots \\ x(k+P\,|k\,) &= f(x(k+P-1),\ g(\Delta u(k+P-1))) \\ &= f(\cdots f(x(k),\ g(\Delta u(k)),\ g(\Delta u(k+M-1))) \end{aligned} \tag{19}$$

where $\xi(k)$ is the state variable at step k; $u(k)$ and $\Delta u(k)$ are the control input and the increment of control input of step k, respectively; $y_c(k)$ is the predicted output at step k; M represents the control horizon in model predictive control. The specific expressions are as follows:

$$\begin{aligned} u\,(k) &= [\delta_f(k)] \\ \Delta u\,(k) &= [\Delta\delta_f(k)] \\ \xi(k) &= [\dot{y}(k), \omega(k), \varphi(k), Y(k), X(k)] \\ y_c(k) &= [\varphi(k), Y(k)] \end{aligned}$$

The optimized problems to be solved in NMPC can be obtained:

$$\begin{aligned} &\min_{U(k)}\ J_{N2DOF}(\bar{\xi}_t, u_t) = \sum_{k=t}^{t+P-1} \Gamma_{yi}[y_c\,(k+1\,|k\,) \\ &\quad - R_e(k+1)]^2 + \Gamma_{ui}\Delta u(k)^2 + J_{t+kT_s} \\ &s.t.\ \xi_{k+1,t} = f^{N2DOF}\left(\xi_{k,t}, u_{k,t}\right) \\ &\quad k = t, \ldots, t+P-1 \\ &\quad y_c(k+1\,|k\,) = [\,0 \quad 0 \quad 1 \quad 1 \quad 0\,] \cdot \xi_{k+1,t} \\ &\quad k = t, \ldots, t+P-1 \\ &\quad u_{k,t} = u_{t+M,t} \\ &\quad k = t+M+1, \ldots, t+P-1 \\ &\quad \Delta u_{k,t} \in [-\Delta u_{\max}, \Delta u_{\max}] \\ &\quad k = t, \ldots, t+M-1 \\ &\quad u_{k,t} \in [-u_{\max}, u_{\max}] \\ &\quad k = t, \ldots, t+P-1 \\ &\quad \xi_{t,t} = \xi(t) \end{aligned} \tag{20}$$

where J_{N2DOF} is the optimized objective function based on the nonlinear 2-DOF model; $\bar{\xi}_t = [\bar{\xi}_{t,t}, \bar{\xi}_{t+1,t}, \ldots, \bar{\xi}_{t+P-1,t}]$ is the sequence including five state variables; $R_e\,(k)$ is the reference value obtained from the sigmoid function at step k, which can be expressed as $R_e\,(k) = [\varphi_{ref}(k), Y_{ref}(k)]$; $u\,(k)$ is the control input at step k; Γ_{yi} and Γ_{ui} are the weighting matrices corresponding to the controlled output and input, respectively.

The cost function is composed of three parts, whose meanings are as follows:

- $J_{N2DOF}1 = \sum_{k=t}^{t+P-1} \Gamma_{yi}[y_c\,(k+1\,|k\,) - R_e\,(k+1)]^2$ indicates that the deviation between the predicted output and reference should be as small as possible. It can be expanded as $\Gamma_{y1}[Y_{k,t} - Y_{refk,t}]^2 + \Gamma_{y2}[\varphi_{k,t} - \varphi_{refk,t}]^2$. Γ_{y1} and Γ_{y2} are the weighting factors corresponding to lateral displacement and yaw angle output, respectively;
- $J_{N2DOF}2 = \sum_{k=t}^{t+P-1} \Gamma_{ui}\Delta u(k)^2$ ensures that the control input increment is as small as possible to make the control action smooth. Γ_{ui} represents the weighting factor corresponding to control input increment;
- $J_{N2DOF}3 = \sum_{k=t}^{t+P-1} J_{t+kT_s}$ represents the risk index between the vehicle and the dynamic obstacle. When the vehicle approaches the obstacle, the weight of this term in the cost function will increase. In this case, collision avoidance will become the primary task for safe driving.

The Fmincon nonlinear programming algorithm of the MATLAB tool is used to solve the above optimization function. After solving the optimal control sequences, the first element is taken as the obtained control input value. Then, rolling horizon repeat optimization is performed. The built-in sequence quadratic program can effectively solve the above optimization problem.

B. VARYING DISCRETE STEPS

In model predictive control, the selection of discrete time will determine the effectiveness and efficiency of the system. In vehicle control, the discrete time should be as small as possible to make the control actions accurate. However, in collision avoidance control, a long prediction distance is expected to predict the future further. If a small discrete time is chosen, more discrete steps will be required. The computational burden of the control system will be increased in this case. On the basis of the above considerations, the method of varying discrete steps is used in accordance with literatures [13], [28], [29].

The prediction horizon consists of two components. A small discrete time $T_{s,short} = 0.01s$ is chosen for the accurate vehicle control comprising of P_1 time steps. Then, a large discrete time $T_{s,long} = 0.1s$ of P-P_1 steps is in the predictive horizon for long distance prediction.

C. STABILITY CONSTRAINT

Lateral acceleration should be constrained to prevent from reaching the limit of tire adhesion.

$$\begin{aligned} &\left|a_y\,(k+i)\right| \le a_{y\max} \quad i = 1, 2 \ldots\ldots P-1 \\ &s.t.\ a_{y\max} = \mu g \end{aligned} \tag{21}$$

where μ is the road adhesion coefficient. The value of a_y at each step k in MPC can be calculated in accordance with equation (8a).

VII. SIMULATION AND RESULTS

The effectiveness of the proposed controller is verified in different situations using MATLAB/Simulink and CarSim. Generally, the longer the predictive horizon P is, the more vehicle dynamic information will be obtained.

However, long predictive horizon will intensify unknown interference and increase the computational burden of NMPC. Likewise, the optimized control action will be smooth when a large control horizon M is selected. However, the optimization efficiency of NMPC will be affected in this case. In this paper, the simulation parameters are shown in Table 1.

TABLE 1. Simulation parameters.

Parameters	Symbol	Value	Unit
Distance from CG to front axle	l_f	1.04	m
Distance from CG to rear axle	l_r	1.56	m
Half width of vehicle	c	0.7	m
Yaw moment of inertia	I_z	2031.4	$kg \cdot m^2$
Vehicle speed	U_0	20	m/s
Road Adhesion Coefficient	μ	0.85	/
Control Horizon	M	1	/
Predictive Horizon	P	10	/
Small discrete step	P_1	4	/
Weight Factor of objective item	Γ_{y1}	3000	/
Weight Factor of objective item	Γ_{y2}	1000	/
Weight Factor of objective item	Γ_{ui}	800	/
Weight Factor of J_{t+kT_s}	K_{obs}	1100	/

To show the reference trajectory tracking effect, two sets of vehicle state curves are given in Figures 10 and 11, respectively. The black and blue solid curves represent the reference and actual tracking values, respectively. Figure 10 shows the comparison of the actual lateral displacement curve with the reference when no obstacles appear on the predefined trajectory. The actual value achieves a maximum of $3m$ at $X = 140m$. As shown in Figure 11, the maximum value of the actual yaw angle is $8.3°$ at $X = 90m$. It can be seen that both the actual maximum lateral displacement and yaw angle can track the reference values well. If new obstacles threaten vehicle safety in actual scenes, then the trajectory should be adjusted dynamically to avoid obstacles. In the following sections, two scenes are listed to verify the effectiveness of the proposed controller.

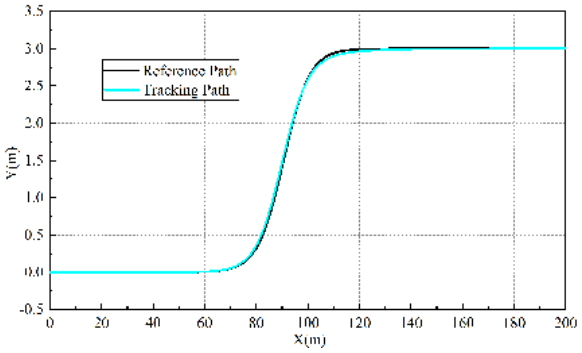

FIGURE 10. Lateral displacement of tracking.

A. SINGLE DYNAMIC OBSTACLE SCENE

In this section, a single dynamic obstacle scene is shown. The simulation time is set to $10s$. When the vehicle travels along the reference trajectory to $X = 100m$, a dynamic obstacle appears at $(140, -1)$ in the geodetic coordinate

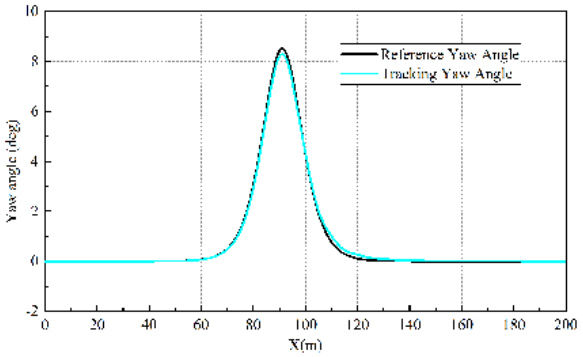

FIGURE 11. Yaw angle of tracking.

system. It moves along the Y-axis at a speed of $2m/s$. In this case, the vehicle will collide with a dynamic obstacle at $X = 140m$ if the reference trajectory is not dynamically adjusted. Dynamic trajectory planning that considers the motion states of obstacles or not in the predictive horizon are obtained, as depicted in Figure 12.

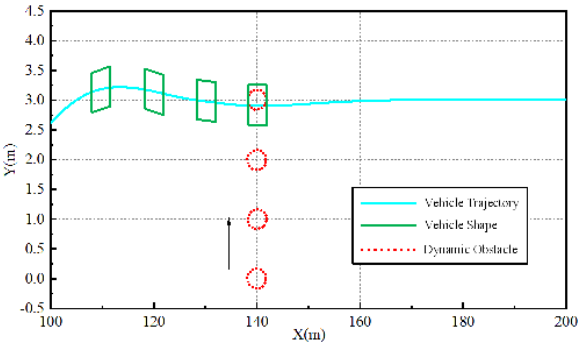

(a) Not considering the motion of the obstacle in the predictive horizon.

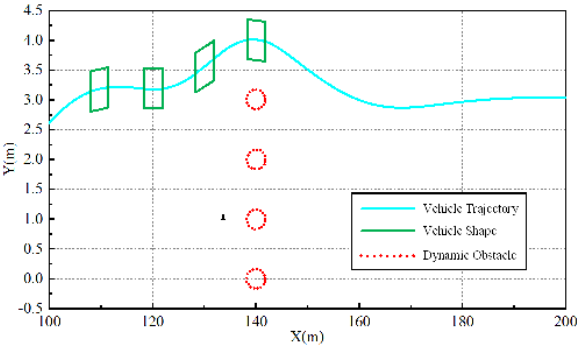

(b) Considering the motion of the obstacle in the predictive horizon.

FIGURE 12. Partial enlargement of the dynamic planned trajectory.

In Figure 12, the blue and green solid curves represent the trajectory and shape of the vehicle, respectively. The red dotted line describes the dynamic obstacle. The vehicle collides with a dynamic obstacle at $X = 140m$ in Figure 12(a). In comparison with Figure 12(a), the motion states of the obstacle are considered in the predictive horizon

in Figure 12(b). The vehicle achieves a maximum lateral displacement of $4m$, thereby avoiding collision with obstacles.

Figure 13 shows the front steering angle considering the dynamic obstacles in the predictive horizon. The vehicle starts turning and tracking the reference trajectory at $t = 3s$ to achieve a lane change operation. At $t = 5.9s$, a new steering operation is implemented to avoid the dynamic obstacle. The front steering angle achieves the maximum and minimum values of $3°$ and $-4°$ at $t = 6.5s$ and $7s$, respectively. Slight jitters can be observed in the curve at $t = 6 - 7s$. Because in this case, obstacle avoidance plays a crucial role, and the discrete step size is $0.1s$ for long distance prediction, thereby affecting controller optimization.

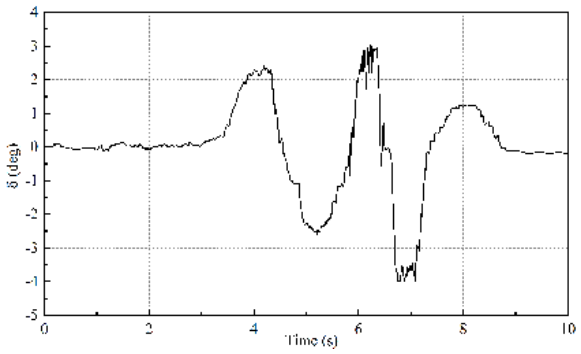

FIGURE 13. Front steering angle of the proposed controller.

Under the effect of the front steering angle shown in Figure 13, the vehicle's state response curves are obtained. As shown in Figure 14(a), the maximum and minimum values of the yaw angle are $7.5°$ and $-3.8°$, respectively. The maximum absolute value of lateral acceleration curve is $5m/s^2$ at $t = 7s$ in Figure 14(b). As shown in Figure 14(c), the maximum absolute value of vehicle slip angle achieves $0.32°$ at $t = 7.6s$. The maximum absolute values of the lateral acceleration and the slip angle are within the stable area. Therefore, the vehicle can maintain stability when avoiding collision.

In Figure 15, the computation burden of the proposed controller at each time step is exhibited. The maximum time of all iteration steps is $0.217s$. The computation efficiency can also ensure the vehicle of avoiding dynamic obstacles.

B. TWO DYNAMIC OBSTACLES SCENE

The scenario in this section considers two dynamic obstacles. The simulation time is set to be $15s$. When the vehicle arrives at $X = 105m$, a dynamic obstacle A is detected at (145, 0) in the geodetic coordinate system. At this moment, it is moving along the Y-axis with an acceleration of $1.5m/s^2$ from a stationary state. In this case, the vehicle should adjust the predefined trajectory to avoid collision with this obstacle. Afterwards, another dynamic obstacle B, with a velocity of $2m/s$ along the X-axis and $1m/s$ along the Y-axis, is detected at (224, 0) when the vehicle drives at $X = 170m$. At this moment, the vehicle should also perform steering operation to avoid it in tracking the predefined trajectory.

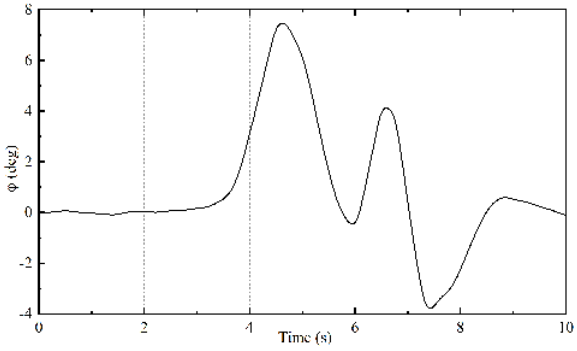

(a) Yaw angle.

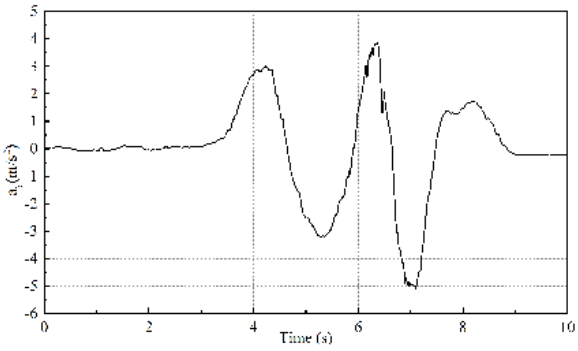

(b) Lateral acceleration.

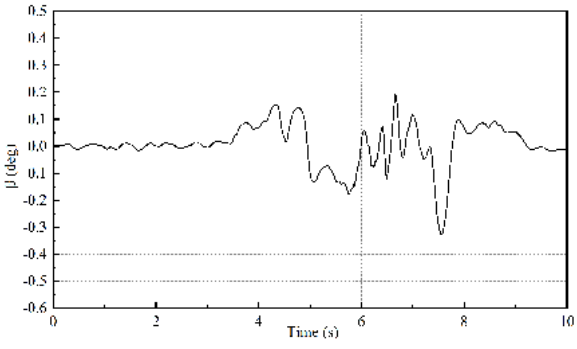

(c) Slip angle.

FIGURE 14. Status response curves of the vehicle.

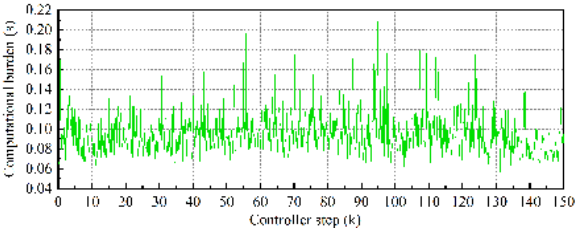

FIGURE 15. Computational burden of the proposed controller.

In Figure 16, two control strategies are adopted to avoid collision. The blue and green solid curves describe the vehicle trajectory and shape, respectively. And the pink and red dotted lines stand for dynamic obstacle A and B, respectively. L_{VH}^X and L_{obs}^X represent the position of vehicle and obstacle under vehicle's longitudinal displacement X, respectively.

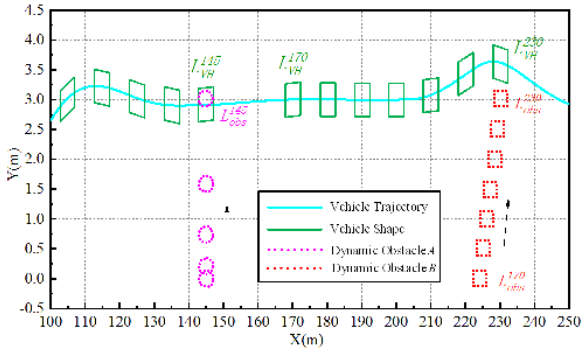

(a) Not considering the motion of the obstacle in the predictive horizon.

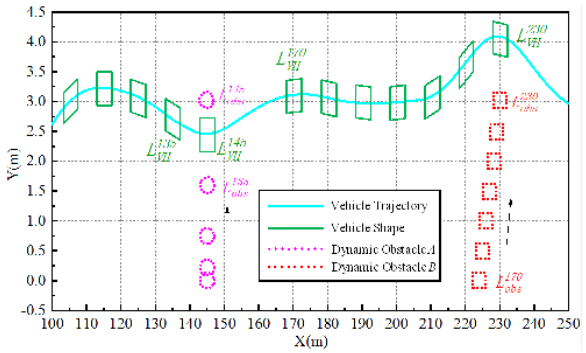

(b) Considering the motion of the obstacle in the predictive horizon.

FIGURE 16. Partial enlargement of the dynamic planned trajectory.

Simulation curve without considering obstacles motion in the predictive horizon is shown in Figure 16(a). It can be seen that the vehicle will collision with obstacle A at $X = 145m$. And there is a lateral deviation between vehicle and obstacle B at $X = 230m$. In this case, collision avoidance optimization has been identified as a failure. Collision phenomenon can be avoided by considering obstacles motion state in the predictive horizon. In Figure 16(b), when the vehicle drives from $X = 130m$ to $X = 160m$, no collision occurs with obstacle A. For obstacle B, the vehicle achieves a lateral displacement of $4m$ to avoid collision at $X = 230m$. Simulation results show that the proposed method can achieve better collision avoidance effect in this scene.

The optimized front steering angle of the proposed controller is exhibited in Figure 17. Before $t = 6s$, the vehicle performs a lane change operation by tracking the reference path. At $t = 6s$, the vehicle starts to turn right to avoid obstacle A. From $t = 10s$ to $t = 12s$, collision avoidance with obstacle B is operated by turning left. The front steering angle reaches its maximum value of $3.2°$ at $t = 10.4s$ and its minimum value of $-4°$ at $t = 11.5s$. Some slight jitters are also found in the curve between $t = 6-7s$ and $t = 10-11s$.

Figures 18(a)-(c) display the state response curves of vehicle. The maximum and minimum values of vehicle yaw angle are $7.5°$ at $t = 4.7s$ and $-4.1°$ and at $t = 12s$, as shown in Figure 18(a). The maximum absolute value of the lateral acceleration curve is $4.9m/s^2$ at $t = 11.6s$, as shown in

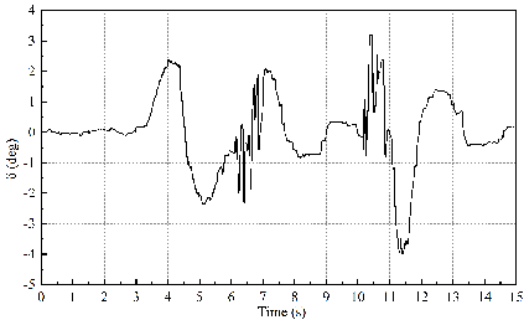

FIGURE 17. Front steering angle of the proposed controller.

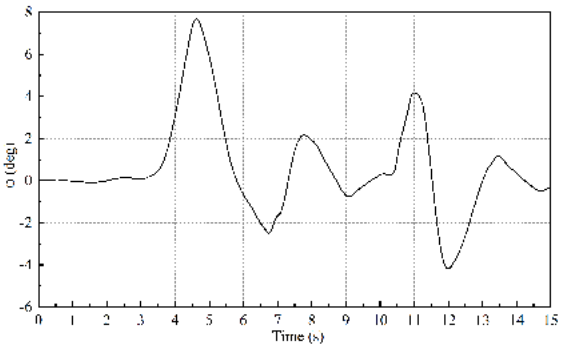

(a) Yaw angle.

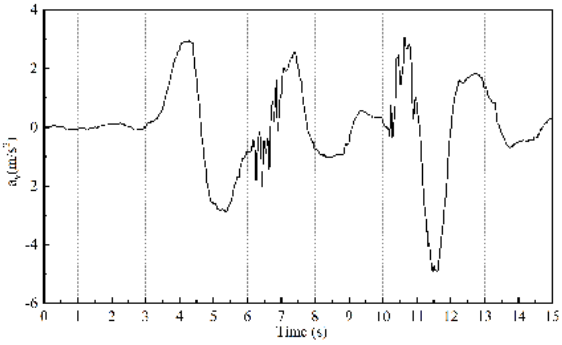

(b) Lateral acceleration.

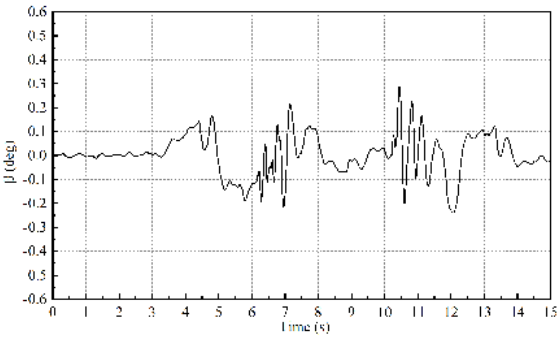

(c) Slip angle.

FIGURE 18. Status response curves of the vehicle.

Figure 18(b). As shown in Figure 18(c), the maximum absolute value of vehicle slip angle achieves $0.3°$ at $t = 10.4s$. The maximum absolute values of the lateral acceleration and slip angle are also within the stability area. The results show

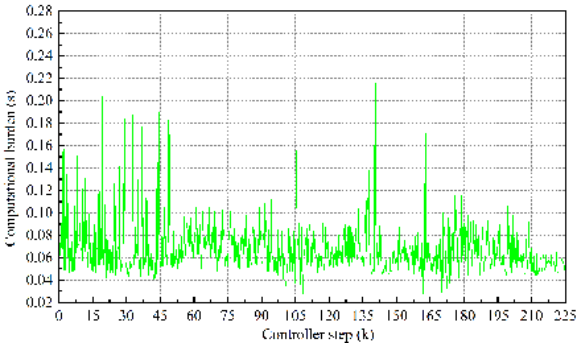

FIGURE 19. Computational burden of the proposed controller.

that the vehicle can ensure driving stability in the process of obstacles avoidance.

The computational burden at each step of the proposed controller is shown in Figure 19. It can be seen that the maximum time of all iteration steps is 0.219*s*. In this study, the optimal problem is solved using the solution tool from the MATLAB toolbox. In the future work, we will exploit the ACADO toolkit and the accompanying code generation tool to reduce actual computational time further.

VIII. CONCLUSION

In this study, an integrated controller is developed for collision avoidance. Simultaneous trajectory dynamic planning and tracking are integrated as a single-level NPMC controller. The reference trajectory is predefined using a sigmoid function. When dynamic obstacles suddenly appear, the trajectory should be dynamically adjusted. Collision avoidance is realized effectively by constructing a moving trend function to predict the obstacle position variances in the predictive horizon. A risk index is constructed to reflect the relative position relationship between vehicle and obstacles in the predictive horizon. Then the designed risk index is introduced into the cost function to realize collision avoidance better. The proposed controller also considers lateral acceleration as vehicle stability constraint. Simulations are conducted under two typical conditions to reveal the effectiveness of the proposed controller. However, sometimes the motion of obstacle is random in actual scenes. In the future, we will consider the random movement of moving obstacles in the predictive horizon. Collision avoidance optimization control based on spatial MPC is also a research direction in the future.

REFERENCES

[1] M. A. Abbas, R. Milman, and J. M. Eklund, "Obstacle avoidance in real time with Nonlinear Model Predictive Control of autonomous vehicles," in *Proc. IEEE 27th Can. Conf. Elect. Comput. Eng. (CCECE)*, May 2014, pp. 1–6.

[2] H. Guo, F. Liu, F. Xu, H. Chen, D. Cao, and Y. Ji, "Nonlinear model predictive lateral stability control of active chassis for intelligent vehicles and its FPGA implementation," *IEEE Trans. Syst., Man, Cybern., Syst.*, vol. 49, no. 1, pp. 2–13, Jan. 2019.

[3] H. Gao, B. Cheng, J. Wang, K. Li, J. Zhao, and D. Li, "Object classification using CNN-based fusion of vision and LIDAR in autonomous vehicle environment," *IEEE Trans. Ind. Informat.*, vol. 14, no. 9, pp. 4224–4231, Sep. 2018.

[4] J. Su, J. Wu, P. Cheng, and J. Chen, "Autonomous vehicle control through the dynamics and controller learning," *IEEE Trans. Veh. Technol.*, vol. 67, no. 7, pp. 5650–5657, Jul. 2018.

[5] X. Na and D. J. Cole, "Application of open-loop stackelberg equilibrium to modeling a driver's interaction with vehicle active steering control in obstacle avoidance," *IEEE Trans. Human-Mach. Syst.*, vol. 47, no. 5, pp. 673–685, Oct. 2017.

[6] U. Rosolia, S. De Bruyne, and A. G. Alleyne, "Autonomous vehicle control: A Nonconvex approach for obstacle avoidance," *IEEE Trans. Control Syst. Technol.*, vol. 25, no. 2, pp. 469–484, Mar. 2017.

[7] K. D. Do, "Synchronization motion tracking control of multiple underactuated ships with collision avoidance," *IEEE Trans. Ind. Electron.*, vol. 63, no. 5, pp. 2976–2989, May 2016.

[8] S. He, M. Wang, S.-L. Dai, and F. Luo, "Leader-follower formation control of USVs with prescribed performance and collision avoidance," *IEEE Trans. Ind. Informat.*, vol. 15, no. 1, pp. 572–581, Jan. 2019.

[9] Z. Peng, D. Wang, T. Li, and M. Han, "Output-feedback cooperative formation maneuvering of autonomous surface vehicles with connectivity preservation and collision avoidance," *IEEE Trans. Cybern.*, to be published.

[10] J. Liu, P. Jayakumar, J. L. Stein, and T. Ersal, "An MPC algorithm with combined speed and steering control for obstacle avoidance in autonomous ground vehicles," in *Proc. ASME Dyn. Syst. Control Conf.*, Jan. 2016. doi: 10.1115/DSCC2015-9747.

[11] J. Liu, P. Jayakumar, J. L. Stein, and T. Ersal, "A double-worst-case formulation for improving the robustness of an MPC-based obstacle avoidance algorithm to parametric uncertainty," in *Proc. Amer. Control Conf. (ACC)*, May 2017, pp. 5562–5567.

[12] J. Liu, P. Jayakumar, J. L. Stein, and T. Ersal, "Combined speed and steering control in high-speed autonomous ground vehicles for obstacle avoidance using model predictive control," *IEEE Trans. Veh. Technol.*, vol. 66, no. 10, pp. 8746–8763, Oct. 2017.

[13] J. Funke, M. Brown, S. M. Erlien, and J. C. Gerdes, "Collision avoidance and stabilization for autonomous vehicles in emergency scenarios," *IEEE Trans. Control Syst. Technol.*, vol. 25, no. 4, pp. 1204–1216, Jul. 2016.

[14] A. Gray, Y. Gao, T. Lin, J. K. Hedrick, H. E. Tseng, and F. Borrelli, "Predictive control for agile semi-autonomous ground vehicles using motion primitives," in *Proc. Amer. Control Conf. (ACC)*, Jun. 2012, pp. 4239–4244.

[15] G. Kahn, A. Villaflor, V. Pong, P. Abbeel, and S. Levine, "Uncertainty-aware reinforcement learning for collision avoidance," 2017, *arXiv:1702.01182*. [Online]. Available: https://arxiv.org/abs/1702.01182

[16] Z. Cao, H. Guo, J. Zhang, F. Oliehoek, and U. Fastenrath, "Maximizing the probability of arriving on time: A practical Q-learning method," in *Proc. 31th AAAI Conf. Artif. Intell. (AAAI)*, Feb. 2017.

[17] J. Ji, A. Khajepour, W. W. Melek, and Y. Huang, "Path planning and tracking for vehicle collision avoidance based on model predictive control with multiconstraints," *IEEE Trans. Veh. Technol.*, vol. 66, no. 2, pp. 952–964, Feb. 2017.

[18] C. Shen, Y. Shi, and B. Buckham, "Integrated path planning and tracking control of an AUV: A unified receding horizon optimization approach," *IEEE/ASME Trans. Mechatronics*, vol. 22, no. 3, pp. 1163–1173, Jun. 2017.

[19] F. Borrelli, P. Falcone, T. Keviczky, J. Asgari, and D. Hrovat, "MPC-based approach to active steering for autonomous vehicle systems," *Int. J. Veh. Auto. Syst.*, vol. 3, nos. 2–4, pp. 265–291, 2005.

[20] H. Guo, F. Liu, R. Yu, Z. Sun, and H. Chen, "Regional path moving horizon tracking controller design for autonomous ground vehicles," *Sci. China Inf. Sci.*, vol. 60, Jan. 2017, Art. no. 013201.

[21] C. E. Beal and J. C. Gerdes, "Model predictive control for vehicle stabilization at the limits of handling," *IEEE Trans. Control Syst. Technol.*, vol. 21, no. 4, pp. 1258–1269, Jul. 2012.

[22] P. Falcone, F. Borrelli, J. Asgari, H. E. Tseng, and D. Hrovat, "Low complexity mpc schemes for integrated vehicle dynamics control problems," in *Proc. 9th Int. Symp. Adv. Vehicle Control*, 2008, pp. 1–6.

[23] Y. Gao, T. Lin, F. Borrelli, E. Tseng, and D. Hrovat, "Predictive control of autonomous ground vehicles with obstacle avoidance on slippery roads," in *Proc. Dyn. Syst. Control Conf.*, Jan. 2011, pp. 265–272.

[24] Y. Gao, A. Grav, J. Frasch, T. Lin, F. Tseng, J. K. Hedrick, and F. Borrelli, "Spatial predictive control for agile semi-autonomous ground vehicles," in *Proc. 11th Int. Symp. Adv. Vehicle Control*, Sep. 2012, pp. 1–6.

[25] Y. Gao, "Model predictive control for autonomous and semiautonomous vehicles," Ph.D. dissertation, Dept. Eng. Mech. Eng., Univ. California, Berkeley, Berkeley, CA, USA, 2014.
[26] H. Febbo, J. Liu, P. Jayakumar, J. L. Stein, and T. Ersal, "Moving obstacle avoidance for large, high-speed autonomous ground vehicles," in *Proc. Amer. Control Conf. (ACC)*, Seattle, WA, USA, May 2017, pp. 5568–5573.
[27] H. Y. Guo, C. Shen, H. Zhang, H. Chen, and R. Jia, "Simultaneous trajectory planning and tracking using an MPC method for cyber-physical systems: A case study of obstacle avoidance for an intelligent vehicle," *IEEE Trans. Ind. Informat.*, vol. 14, no. 9, pp. 4273–4283, Mar. 2018.
[28] S. M. Erlien, S. Fujita, and J. C. Gerdes, "Shared steering control using safe envelopes for obstacle avoidance and vehicle stability," *IEEE Trans. Intell. Transp. Syst.*, vol. 17, no. 2, pp. 441–451, Feb. 2016.
[29] M. Brown, J. Funke, S. Erlien, and J. C. Gerdes, "Safe driving envelopes for path tracking in autonomous vehicles," *Control Eng. Pract.*, vol. 61, pp. 307–316, Apr. 2017.
[30] S. Lefevre, D. Vasquez, and C. Laugier, "A survey on motion prediction and risk assessment for intelligent vehicles," *ROBOMECH J.*, vol. 1, no. 1, p. 1, Jul. 2014.
[31] M. Castillo-Lopez, S. A. Sajadi-Alamdari, J. L. Sanchez-Lopez, M. A. Olivares-Mendez, and H. Voos, "Model predictive control for aerial collision avoidance in dynamic environments," in *Proc. 26th Medit. Conf. Control Automat. (MED)*, Zadar, Croatia, Jun. 2018, pp. 1–6.
[32] N. Yuuki, N. Kenichiro, and S. Kazuma, "Moving obstacle avoidance control by fuzzy potential method and model predictive control," in *Proc. 11th Asian Control Conf. (ASCC)*, Gold Coast, QLD, Australia, Dec. 2017, pp. 1298–1303.
[33] Z. Wang, G. Li, H. Jiang, Q. Chen, and H. Zhang, "Collision-free navigation of autonomous vehicles using convex quadratic programming-based model predictive control," *IEEE/ASME Trans. Mechatronics*, vol. 23, no. 3, pp. 1103–1113, Jun. 2018.
[34] T. Weiskircher, Q. Wang, and B. Ayalew, "Predictive guidance and control framework for (Semi-)autonomous vehicles in public traffic," *IEEE Trans. Control Syst. Technol.*, vol. 25, no. 6, pp. 2034–2046, Nov. 2017.
[35] W. Qian, A. Beshah, and W. Thomas, "Predictive maneuver planning for an autonomous vehicle in public highway traffic," *IEEE Trans. Intell. Transp. Syst.*, vol. 20, no. 4, pp. 1303–1315, Apr. 2019.
[36] M. G. Plessen, D. Bernardini, H. Esen, and A. Bemporad, "Spatial-based predictive control and geometric corridor planning for adaptive cruise control coupled with obstacle avoidance," *IEEE Trans. Control Syst. Technol.*, vol. 26, no. 1, pp. 38–50, Jan. 2018.
[37] C. Ackermann, J. Bechtloff, and R. Isermann, "Collision avoidance with combined braking and steering," in *Proc. 6th Int. Munich Chassis Symp.* Wiesbaden, Germany: Springer Fachmedien Wiesbaden, 2015, pp. 199–213.
[38] R. Liu and J. Duan, "A path tracking algorithm of intelligent vehicle by preview strategy," in *Proc. 32nd Chin. Control Conf.*, Jul. 2013, pp. 5630–5635.
[39] J. Liu, P. Jayakumar, J. L. Stein, and T. Ersal, "A study on model fidelity for model predictive control-based obstacle avoidance in high-speed autonomous ground vehicles," *Vehicle Syst. Dyn*, vol. 54, no. 11, pp. 1629–1650, Nov. 2016.
[40] Y. Yoon, J. Shin, H. J. Kim, Y. Park, and S. Sastry, "Model-predictive active steering and obstacle avoidance for autonomous ground vehicles," *Control Eng. Pract.*, vol. 17, no. 7, pp. 741–750, Jul. 2009.

SHAOSONG LI received the Ph.D. degree in automotive engineering from Jilin University, Jilin, China, where he focused on vehicle dynamics and control.

He is currently the Director of the Vehicle Engineering Department, Changchun University of Technology. His current research interests include the application of control systems to vehicle dynamics to improve safety, stability, and performance of vehicles in conjunction with human drivers.

Dr. Li is a member of the Society of Automotive Engineers of China. He was a recipient of the Jilin Province Science and Technology Found for Young Scholars and the Ministry of Education Chun hui Plan.

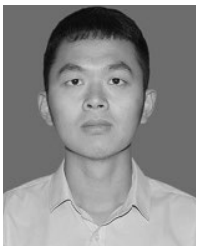

ZHENG LI received the bachelor's degree in automotive engineering from the Heilongjiang Institute of Technology, Heilongjiang, China. He is currently pursuing the master's degree in automotive engineering with the Changchun University of Technology, Jilin, China.

His research interest includes the theory and technology of automotive safety and model predictive control.

ZHIXIN YU received the Ph.D. degree in automotive engineering from Jilin University, Jilin, China, where he focused on heavy duty vehicle rollover detection and active roll control.

He is currently a Teacher with the Changchun University of Technology. His current research interests include the application of control systems to vehicle dynamics to improve stability and the rollover stability analysis of tank vehicles.

BANGCHENG ZHANG received the B.Eng. and M.Eng. degrees from the Changchun University of Technology, Changchun, China, in 1995 and 2004, respectively, and the Ph.D. degree from Jilin University, Changchun, China, in 2011.

He is currently a Professor with the Changchun University of Technology. He has been an Academic Visitor with Tsinghua University, Beijing, China, in 2007. He has published about 20 articles. His research interests include mechatronics measurement technique and fault diagnosis.

NIAONA ZHANG received the Ph.D. degree. She is currently a Professor, the Head of the RD and Innovation Team for Key Technologies of Electric Vehicle and Chassis Control, Jilin, and the Director of the Engineering Research Center for Complex Electromechanical Equipment Technology, Jilin. She has published two academic monographs, more than 50 articles on academic journals and international academic conferences, and eight of her published patents were authorized. Her research interests include the electric vehicle drive theory and control technology, complex system modeling, and optimization and control. She carried out and accomplished 16 provincial and municipal scientific research programs and achieved six provincial and ministerial awards for scientific and technological progress as the first accomplisher.